

Article

Cationic Dye Adsorption on Hydrochars of Winery and Citrus Juice Industries Residues: Performance, Mechanism, and Thermodynamics

Nepu Saha ¹, Maurizio Volpe ² , Luca Fiori ^{3,4} , Roberto Volpe ⁵ , Antonio Messineo ² 
and M. Toufiq Reza ^{1,*} 

¹ Department of Biomedical and Chemical Engineering and Sciences, Florida Institute of Technology, Melbourne, FL 32901, USA; nsaha2019@my.fit.edu

² Faculty of Engineering and Architecture, University of Enna KORE, 94100 Enna, Italy; maurizio.volpe@unikore.it (M.V.); antonio.messineo@unikore.it (A.M.)

³ Department of Civil, Environmental and Mechanical Engineering, University of Trento, 38123 Trento, Italy; luca.fiori@unitn.it

⁴ Center Agriculture Food Environment (C3A), University of Trento, 38010 San Michele all'Adige (Trento), Italy

⁵ School of Engineering and Materials Science, Queen Mary University of London, London E1 4NS, UK; r.volpe@qmul.ac.uk

* Correspondence: treza@fit.edu; Tel.: +1-321-674-8578

Received: 11 August 2020; Accepted: 7 September 2020; Published: 9 September 2020



Abstract: With the increasing needs of clean water supplies, the use of biomass wastes and residues for environmental remediation is essential for environmental sustainability. In this study, the residues from winery and citrus juice industries, namely grape skin and orange peel, respectively, were first converted to hydrochars by hydrothermal carbonization (HTC) and then a cationic dye (methylene blue) adsorption was studied on hydrochars. Hydrochars from both feedstocks were produced at three different temperatures (180, 220, and 250 °C) and a fixed residence time (1 h) to evaluate the hydrochar's performance on the dye adsorption. The hydrochars were characterized in terms of their pH, pH at point of zero charge (pH_{PZC}), surface functionalities, and surface area. A batch adsorption study of the dye was carried out with variable adsorbate concentration, pH, and temperature. Two adsorption isotherms namely Langmuir and Freundlich models were fitted at 4, 20, and 36 °C. The thermodynamic properties of adsorption (Gibbs free energy (ΔG), enthalpy (ΔH) and entropy (ΔS)) were evaluated from the isotherms fittings. Results showed that the dye adsorption on both hydrochars was significant and followed Langmuir isotherm. The maximum adsorption capacity on citrus waste hydrochar was higher than the winery waste hydrochar at any corresponding HTC temperature. Although hydrochars showed the lowest surface area (46.16 ± 0.11 and 34.08 ± 1.23 m²/g for citrus and winery wastes, respectively) at 180 °C, their adsorption was the highest, owing to their maximum density of total oxygen functional groups (23.24 ± 0.22 and 32.69 ± 1.39 $\mu\text{mol}/\text{m}^2$ for citrus and winery wastes, respectively), which decreased with the increase in HTC temperature. This research shows a sustainable route for the production of highly effective adsorbent materials at lower HTC temperatures from citrus and winery wastes.

Keywords: hydrochar; orange peel; grape skin; cationic dye; thermodynamic properties; Boehm titration

1. Introduction

Biomass residues primarily consist of agricultural and agro-industrial wastes that are often discarded during processing. They could be an alternative source of energy or represent value-added

materials [1,2]. In fact, one of the key factors of developing a circular economy is the efficient valorization of agricultural and agro-industrial wastes, such as sunflower stems, walnut shells, olive stones, palm empty fruit bunches, orange peel, and grape skin. In particular, most of the orange peel waste comes from the citrus industry which is commonly known as citrus waste (CW) while the grape skin waste is from the winery which is also known as winery waste (WW). In 2018, the global productions of orange and grape were 53.2 and 77.8 million megagrams, respectively [3,4]. A substantial amount of these fruits went directly to the industries for juice and wine processing, respectively. After processing, around 50–60% of oranges end up as waste that contains seed, peel, and segment membrane; whereas around 25% of the grape ends up as waste composed of skin, seeds, and stalks [5–8]. Now, grapes skin is a rich source of phenolic compounds (both flavonoids and non-flavonoids) and has a very high sugar content [9]. On the other hand, orange peel is acidic. Both wastes are wet and contain a significant amount of moisture. As a result, the use of these wastes directly as fuel and soil improver is economically unfavorable. Therefore, the advancement of the conversion techniques of the aforementioned wet wastes into valuable materials, such as adsorbents, reduce the environmental liability from juice and winery industries [10,11].

Hydrothermal carbonization (HTC) is a wet process that converts organic wastes into a carbon-rich material, often called hydrochar [12,13]. The reaction temperature varies between 180–260 °C with pressure above the water's saturation pressure. Under this experimental condition, water shows more reactive characteristics due to its high ionic product; at the same time, it behaves as a non-polar solvent as its dielectric constant is low [14]. As a result, biomass undergoes simultaneous reactions of hydrolysis, dehydration, decarboxylation, condensation, polymerization, and aromatization of the original precursor, which produces hydrochar, a solid spherical particle [15,16]. Hydrochar is mesoporous with particle size ranging up to 50 µm. It also contains a low-oxygen hydrophobic core, but with abundant oxygen functional groups on the surface [17,18]. Despite having a relatively low surface area of hydrochar compared to biochars and activated carbons [19,20], these oxygen functional groups improve the chemical reactivity and make it a potential adsorption material [18,21,22].

Until now, most of the hydrochars obtained from CW and WW have been investigated for low-cost solid fuel [13,23]. This is because the higher heating value (HHV) of the hydrochar increases and becomes similar to low-grade coal with the increase in HTC temperature and residence time. Previously reported maximum HHV was 27.6 MJ/kg at 250 °C and 8 h residence time, where the HHV of grape skin raw was 18.7 MJ/kg [23]. However, the economics of fuel production from these wet wastes and their combustibility are still challenging compared with the current low price of coal, natural gas, and crude oil [24,25]. Although fuel characteristics of the hydrochars produced from CW and WW have been previously investigated [12,13,23,26], their use in applications, such as adsorption or soil amendment, fall short in the literature. Recently, researchers have been moving forward to use CW and WW as adsorbents for removing pollutants (e.g., dye, mercury, oil, organic solvent) from water [23,27–31]. For instance, Nascimento et al. investigated the dye adsorption capacity of raw orange peel and found that it can adsorb a maximum of 4.0, 8.7, and 19.6 mg/g of Remazol Yellow Gold, Reactive Gray, and Reactive Turquoise dye, respectively at 25 ± 2 °C [27]. Fernandez et al. studied the adsorption capacity of thermally (underflows of COR₂R) and chemically (with phosphoric acid) activated orange peel hydrochars, where they produced hydrochar at a single temperature of 200 °C [28]. Basso et al. and Purnomo et al. studied the physicochemical properties of hydrochars from grape skin and seeds obtained at 180, 220, and 250 °C [23,29]. Despite some amount of literature on HTC of CW and WW, the effect of HTC conditions on the performance of their hydrochars as adsorbent, adsorption mechanism and thermodynamics is still not well understood [32].

Therefore, the main objective of this study was to evaluate the dye adsorption potential of hydrochars produced from CW and WW at various HTC temperatures. The feedstocks used in this study are not new; however, the effect of HTC temperature on their adsorption capacity is a novelty of this study. Hence, the factors which affect adsorption, such as surface area, surface functionality, acidity or basicity (pH), and the pH at point of zero charge (pH_{PZC}) of the hydrochars were investigated.

In addition to physicochemical characteristics, equilibrium adsorptions were also evaluated at three different adsorption temperatures, such as 4, 20, and 36 °C to determine the thermodynamic parameters of a cationic dye (methylene blue) adsorption. This study allows us to better understand the mechanism and thermodynamics behind the dye adsorption on CW and WW hydrochars in order to estimate their possible application in dye removal from water.

2. Materials and Methods

2.1. Materials

The wet CW (orange peel) was provided by the Misitano and Stracuzzi citrus juices and essential oils factory located in Messina province, Sicily, Italy, while the WW (grape skin) was collected from a wine-production plant at Trentino, Italy. The freshly collected CW and WW wastes were wet and content 78 and 70 wt.% moisture, respectively. These wet feedstocks were dried overnight in an oven at 105 °C. Dried CW and WW were milled, sieved to particle size lower than 800 µm, stored in plastic bags, and put them into a desiccator until use.

Different types of acid and bases were used to perform Boehm titration, which were purchased from various suppliers. For instance, 0.01 N hydrochloric acid (HCl) and 0.01 N sodium hydroxide (NaOH) solutions were purchased from Fisher Scientific, while 0.1 M sodium bicarbonate (NaHCO₃) and 0.1 M sodium carbonate (Na₂CO₃) solutions were purchased from Sigma Aldrich. In order to measure the pH_{PZC}, 99 wt.% potassium nitrate (KNO₃) salt was purchased from Alfa Aesar. A cationic dye, 1% (w/v) methylene blue was purchased from Fisher Scientific to be used in this adsorption study. The dye was diluted as per requirement by using deionized (DI) water.

2.2. HTC Experimental Methods

A 2L AISI 316 stainless steel (SS) reactor was used to perform all the HTC experiments. For each experiment, biomass to DI water ratio was maintained at 1:5 wt/wt and the mixture was placed in the reactor. For instance, 200 g CW and 120 g WW were mixed with 1000 g and 600 g DI water, respectively to maintain the biomass to DI water ratio 1:5 wt/wt. Prior to each experiment, the reactor was purged with nitrogen gas to remove the existing air in the reactor. While the reactor temperature reached its set temperature (180 or 220 or 250 °C), the time count starts. As soon as the residence time of 1 h was over, the reactor was placed on a SS block at −30 °C and blowing air on it for cooling down the reactor. Each time, heating and cooling took about 15–20 min. When the reactor reached room temperature (~25 °C), it was depressurized by allowing the produced gases vented through a water-filled graduated cylinder, thus allowing to measure the produced gas volume. Then, the reactor was opened and the content of the reactor was filtered and the solid product was collected. The wet hydrochar was kept in an oven and dried overnight at 105 °C. All the dried hydrochars were stored in air sealed vials for further analyses. The hydrochar yield was calculated via Equation (1), in terms of the amount of dry solid recovered from the experiment with respect to the amount of dry feedstock initially loaded into the reactor. The mass balance of the HTC experiments is shown in Table 1. The hydrochars were named as CW-HT and WW-HT, where CW stands for orange peel, WW stands for grape skin, H is for HTC treatment, and T is for HTC reaction temperature.

$$\text{Hydrochar yield (\%)} = \frac{\text{Mass of dry hydrochar}}{\text{Mass of dry feedstock initially loaded}} \times 100\% \quad (1)$$

Table 1. Mass balance of hydrothermal carbonization (HTC) experiments.

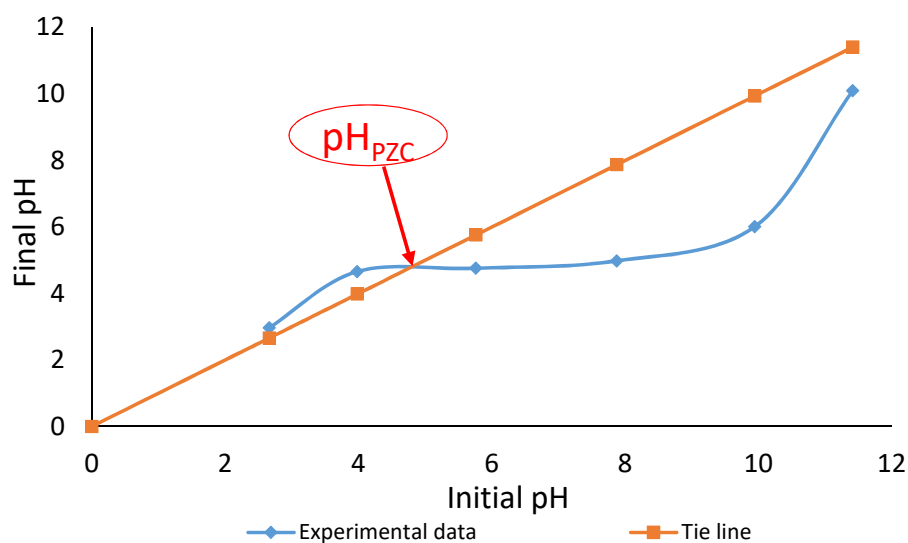
Sample ID	Solid Yield (%)	Liquid Yield (%)	Gas Yield (%)
CW-H180	47.4	49.4	3.2
CW-H220	46.8	49.4	3.8
CW-H250	42.8	48.6	8.5
WW-H180	69.0	28.7	2.3
WW-H220	64.3	31.4	4.3
WW-H250	57.3	36.0	6.7

2.3. Characterization of Solid Products

In this study, the pH of the hydrochar was measured to identify whether the hydrochar was acidic or basic in nature. Furthermore, measuring the pH_{PZC} allowed us to understand whether the hydrochar contained positive, negative, or neutral charges. In addition, the qualitative and quantitative presence of oxygen functional groups was investigated by Fourier-Transform Infrared (FTIR) spectroscopy and Boehm titration, respectively.

A Fisher Scientific pH probe (AE 150) was used to measure the pH of the hydrochar surface. Prior to measure the pH of hydrochar, the sample was thoroughly washed with DI water until a constant pH of the washed water. The washed sample was placed in an oven and dried overnight at 105 °C. This was done to wash off any remaining process liquid (if any) on the hydrochar's surface. The washed dried hydrochar was finally used to measure the pH. Details of this measurement technique are discussed elsewhere [18].

There are several techniques, such as mass titration, potentiometric titration, immersion technique, and pH drift method to measure the pH_{PZC} on a solid surface [33]. Among those techniques, pH drift method was used to measure the pH_{PZC} in this study because it was found to be the most commonly used and reliable method in our earlier studies [18,34]. According to this method, around 0.25 g of dried hydrochar sample was placed in six Erlenmeyer flasks. A 30 mL of pH adjusted (2 to 12 with an interval of 2) 0.03 M KNOR_3R solution was added into each flask and agitated them at 250 rpm for 24 h using an orbital shaker. Final pHs of the solutions were measured after the residence time was over. A plot was drawn by using the initial pH placed in the x-axis and final pH placed on the y-axis. A tie line was drawn in the same axis, where the final pH was considered equal to the initial pH. The intersecting point between those two lines was recognized as pH_{PZC} (see Figure 1). Each of the measurements was duplicated to evaluate reproducibility.

**Figure 1.** pH_{PZC} determination technique using pH drift method.

The Brunauer, Emmett, and Teller (BET) surface area of the hydrochar was measured using a high-pressure volumetric analyzer (Micromeritics HPVA II, Norcross, GA, USA). The BET surface area was calculated using a five-point measurement technique where a linear isotherm plot was considered up to the relative pressure (P/P_0) of 0.3. Ultra-pure N_2 gas was used as the adsorption medium in this study.

Standard Boehm titration methods were used to quantify the oxygen-containing acidic functional groups (OCAFGs) and basic functional groups (BFGs) on the surface of hydrochars [35]. An automatic titrator (Mettler Toledo, T50, Columbus, OH, USA) was used to perform all the titrations. As per the Boehm titration, there are two methods: (i) backward and (ii) forward titration method. A backward titration method was used to measure the OCAFGs, while the forward method was used to measure the BFGs. Detailed experimental procedures including calculation techniques of these methods are discussed elsewhere [36,37].

A Perkin Elmer Spectrum 400 FT-IR/NIR spectrometer (Perkin Elmer Inc., Tres Cantos, Madrid, Spain) was used to identify the presence of primary organic compounds on the hydrochars. The operating conditions were set at the wavenumber range from 600 to 4000 cm^{-1} , with a resolution of 4 cm^{-1} , and 16 scans. All spectra were baseline corrected and normalized.

2.4. Adsorption Methods

Adsorption tests were performed in a set of 15 mL vials, where approximately 25 mg of dry hydrochar samples were placed. An equal volume of 10 mL of dye solutions with initial concentrations of 10–500 mg/L was added into the vials. All the vials were placed in a tube revolver and shake them at 40 rpm and 20 °C for 24 h to reach equilibrium. Similar procedures were followed for the other two sets of vials containing the same initial dye concentrations and the same amount of hydrochars but kept at different temperatures: 4 and 36 °C. All samples were filtered prior to analysis, in order to minimize interference of the fine particles during the analysis. The dye concentrations in the filtered solutions were determined using a Hach-6000 UV–vis spectrometer (Loveland, CO, USA) at 665 nm. The equilibrium adsorption capacity was calculated using Equation (2).

$$q_e = \frac{(C_0 - C_e)V}{W} \quad (2)$$

where,

q_e = equilibrium adsorption capacity in mg/g

C_0 = initial dye concentration in mg/L

C_e = equilibrium dye concentration in mg/L

V = volume of the dye solution in mL, and

W = mass of dry hydrochar used the experiment in g.

The adsorption isotherm of this study was fitted on Langmuir and Freundlich isotherm models shown in the following Equations:

$$q_e = \frac{Q_{max}K_L C_e}{1 + K_L C_e} \quad (3)$$

$$q_e = K_F (C_e)^{1/n_F} \quad (4)$$

where,

Q_{max} = maximum adsorption capacity in mg/g

K_L = Langmuir isotherm coefficient

K_F and n_F = Freundlich adsorption constants

The linear forms of the Langmuir's and Freundlich's isotherm models are shown in Equations (5) and (6). The applicability of the isotherm models to the adsorption experimental data was evaluated considering their correlation R^2 values.

$$\frac{C_e}{q_e} = \frac{1}{Q_{max}K_L} + \frac{C_e}{Q_{max}} \quad (5)$$

$$\ln q_e = \ln K_F + \frac{1}{n_F} \ln C_e \quad (6)$$

In order to determine the progression of adsorption, separation factor (R_L), a dimensionless constant as was calculated by using the following Equation:

$$R_L = \frac{1}{1 + C_0K_L} \quad (7)$$

The variation of the dimensionless parameter, R_L indicates different adsorption scenario as per the following Equation:

$$R_L = \begin{cases} \text{reversible} & \text{if } R_L = 0 \\ \text{favorable} & \text{if } 0 < R_L < 1 \\ \text{linear} & \text{if } R_L = 1 \\ \text{unfavorable} & \text{if } R_L > 1 \end{cases} \quad (8)$$

The thermodynamic properties, such as Gibbs energy (ΔG), enthalpy (ΔH), and entropy (ΔS) were obtained by using the well-known van't Hoff equation and thermodynamic relationship shown in the following Equation:

$$\ln K_c = \frac{\Delta S}{R} - \frac{\Delta H}{RT} \quad (9)$$

$$\Delta G = \Delta H - T\Delta S \quad (10)$$

where, R (8.314 J/mol K) is the universal gas constant, T (K) is the absolute temperature, K_c is the equilibrium constant which must be dimensionless. The K_c can be easily derived by multiplying the Langmuir constant (K_L) by the molecular weight of methylene blue (319.85 g/mol), 1000, and the number of moles of pure water (55.5) per liter [38,39]. Equation (9) is known as van't Hoff equation where the values of ΔH and ΔS were determined from the slope and the intercept of the linear plot of $\log(K_c)$ vs. $1/T$. These values were used to calculate ΔG as shown in Equation (10).

The effect of the solution's pH on dye adsorption capacity was measured by adding 10 mL of 300 mg/L dye solution at various pH of 3–11 with approximately 25 mg of hydrochar sample. The pH of the dye solution was maintained by using 0.01 N HCl and 0.01 N NaOH solutions. The equilibrium adsorption capacity, q_e (mg/g) was calculated by using Equation (2).

3. Results and Discussion

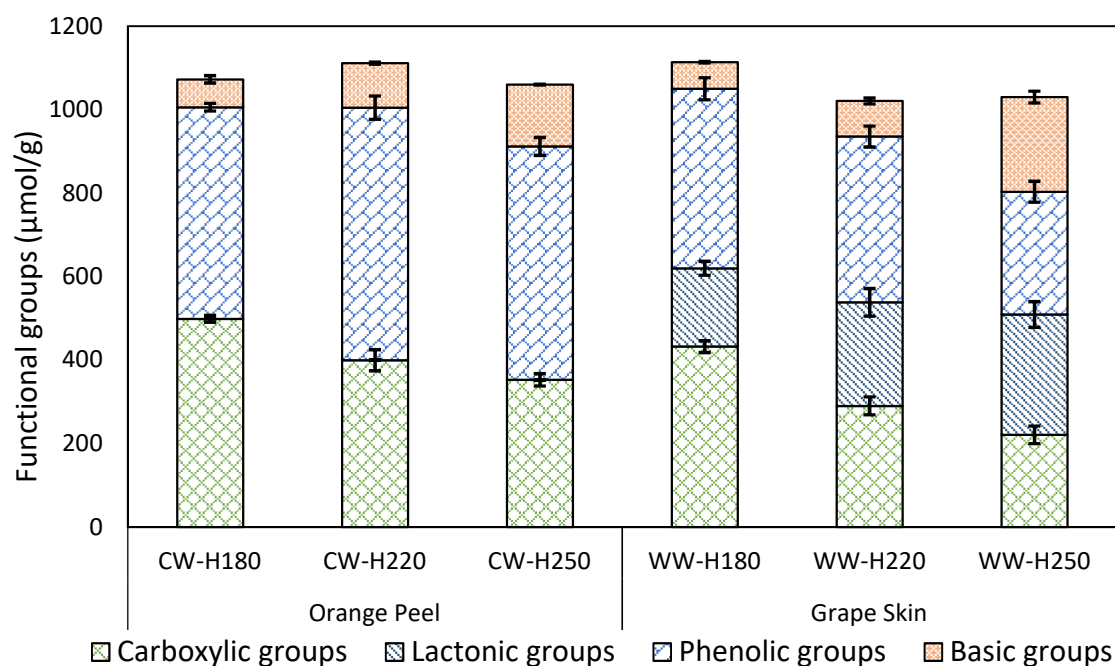
3.1. Physico-Chemical Characteristics of Hydrochar

The chemical state of the hydrochar was characterized by the pH, while the electrical state was characterized by the pH_{PZC} . The pH and pH_{PZC} values of the hydrochar samples are shown in Table 2. The results show that both pH and pH_{PZC} increased with the increase in treatment temperature for both CW and WW. However, CW hydrochar showed a minimal difference in pH and pH_{PZC} , while WW showed higher pH compared to its pH_{PZC} at all conditions. According to the literature, the surface of the hydrochar is typically negatively charged when the pH is higher than its pH_{PZC} and it is positively charged if the pH is lower than its pH_{PZC} [36], which indicates that the WW hydrochars are negatively charged while CW hydrochars are mostly neutral.

Table 2. Physiochemical properties of hydrochars produced from citrus and winery wastes.

Sample ID	pH	pH _{PZC}	BET Surface Area (m ² /g)	Density of Surface Functional Groups (μmol/m ²)
CW-H180	4.74 ± 0.06	4.72 ± 0.15	46.16 ± 0.11	23.24 ± 0.22
CW-H220	5.24 ± 0.05	5.29 ± 0.08	47.60 ± 0.90	23.36 ± 0.51
CW-H250	5.68 ± 0.02	5.61 ± 0.04	63.82 ± 2.08	16.61 ± 0.59
WW-H180	4.72 ± 0.06	4.22 ± 0.06	34.08 ± 1.23	32.69 ± 1.39
WW-H220	6.52 ± 0.08	5.41 ± 0.04	41.96 ± 0.88	24.33 ± 0.54
WW-H250	6.91 ± 0.11	5.67 ± 0.06	48.04 ± 1.61	21.45 ± 0.81

Furthermore, Figure 2 provides quantitative information on the acidic and basic groups on the hydrochars' surfaces. It is observed that the total oxygen functional groups (acidic and basic) on hydrochar surfaces did not vary significantly. Surprisingly, with a deeper look at the specific functional groups, it was observed that acidic oxygen functional groups decreased with HTC temperature and basic oxygen functional groups increased with HTC temperature. As a result, the overall sum of oxygen functional groups remains similar to the increase in HTC temperature. For instance, the carboxylic groups decreased from 499 μmol/g on CW-H180 to 353 μmol/g on CW-H250, while on WW they decreased from 433 μmol/g to 221 μmol/g. The basic functional groups increased with the HTC temperature for both samples. On CW, they increased from 67 to 148 μmol/g and, correspondingly, from 64 to 227 μmol/g for WW. Although no lactonic groups were found in CW samples which is similar to the cellulose and their hydrochar produced at low temperatures studied by Saha et al. [18], the WW samples showed an increasing trend with the HTC temperature.

**Figure 2.** Oxygen-containing functional groups on hydrochars produced from citrus and winery wastes.

This is confirmed by the FTIR spectra shown in Figure 3, where no peak for aliphatic ketone at 1705–1725 cm⁻¹ appeared on CW hydrochars but it appeared on WW-H180 and stayed more visible at higher temperatures (220 and 250 °C). By contrast, the phenolic groups showed an opposite trend whereby they increased for CW sample from 507 to 560 μmol/g but decreased for WW samples from 430 to 294 μmol/g at 180 and 250 °C, respectively. In general, any carbon material contains both acidic and basic properties. However, the dominant property is highly dependent on the pH_{PZC} of that material. While the pH_{PZC} of carbon material is less than 7.0, the material should be dominated by the

acidic groups, otherwise, the basic groups should dominant [40]. The measured pH_{PZC} values are following the domination of total acidic and basic groups in this study.

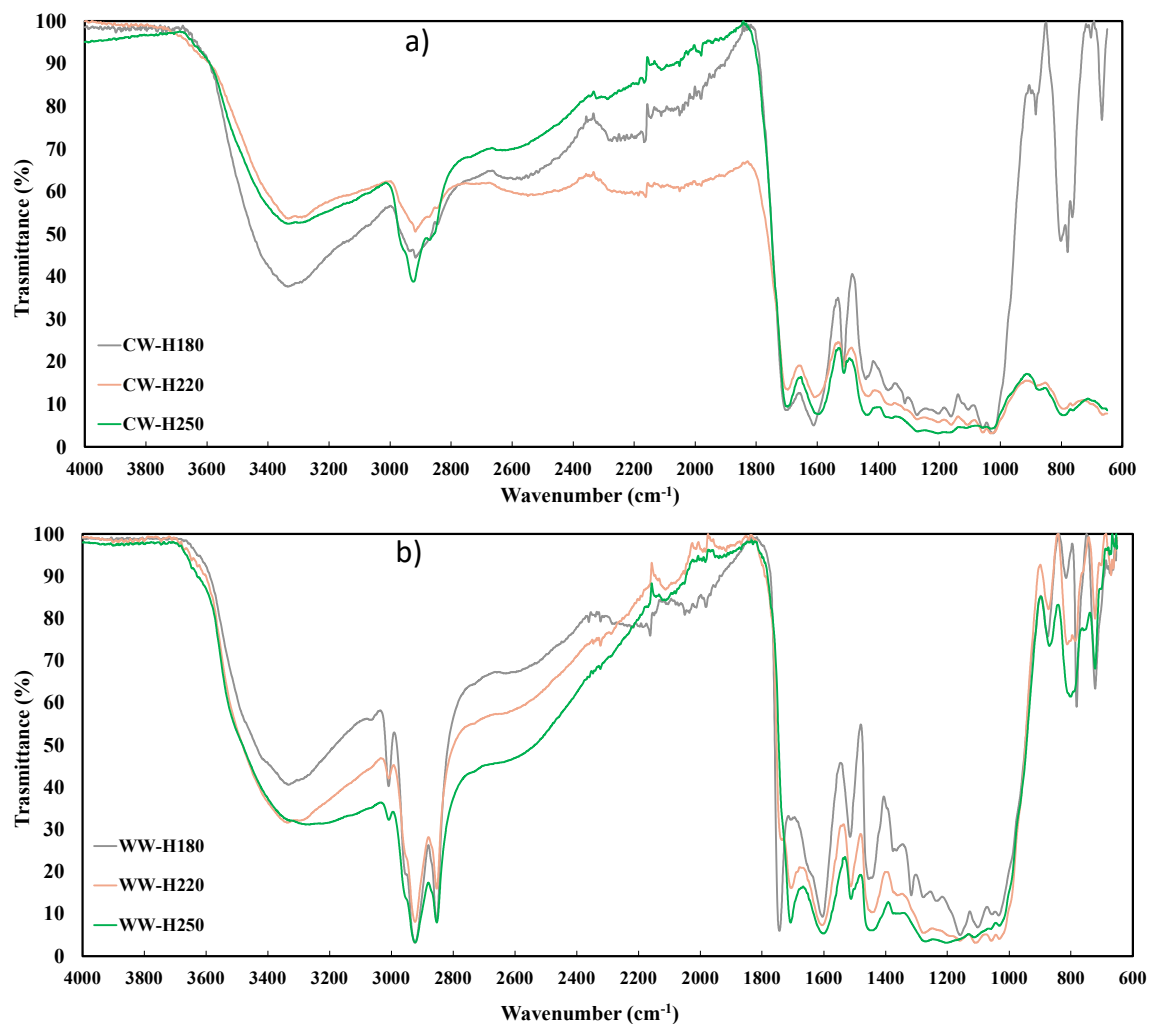


Figure 3. FTIR spectra of hydrochars produced from (a) citrus waste, (b) winery waste.

The BET surface areas of the hydrochars are shown in Table 2. Both CW and WW hydrochars showed an increased surface area with increasing HTC temperature which is an order of magnitude higher than the surface area of the raw feedstock reported in Arslan et al. [41]. This could be related to the removal of volatiles from hydrochars at high-temperature HTC. As the surface area increased and the total functional groups remained almost unchanged, the density of functional groups decreased significantly. The density of functional groups of material represents the number of active sites present per unit surface area. The density of functional groups was $23.24 \mu\text{mol}/\text{m}^2$ on CW-H180 which was reduced to $16.61 \mu\text{mol}/\text{m}^2$ on CW-H250, while this number was reduced from 32.69 to $21.45 \mu\text{mol}/\text{m}^2$ for WW hydrochar at 180 and 250 °C, respectively. The density of functional groups could play an important role if the mechanism of adsorption is of the monolayer type.

3.2. Effect of Solution's pH on Adsorption

The pH of the solution highly affects the surface charge of the adsorbent, which ultimately controls the adsorption process. The effect of the initial pH of the solution in a range of 3 to 11 was studied for the removal of dye by hydrochar samples as shown in Figure 4. The results indicate that the solution's pH significantly affects the adsorption, particularly under the highest alkaline condition ($pH = 11$) for

both types of hydrochars. The adsorption capacity was found slightly lower in the acidic environment compared to the neutral condition. Although the adsorption remained more or less similar at pH 8 and 10, it increased around 3 to 4 times at pH 11 compared to the amount adsorbed at pH 7. The reason could be the ion exchange between the hydrochar surface and the cationic dye molecule. At lower initial pH values (3–6), the solution contains an excess amount of hydrogen ions (H^+) which competed with the cationic dye to attack the active sites of the hydrochar. Due to the competition of finding active sites, a decrease in adsorption was observed at lower initial pHs. On the other hand, at higher initial pH (>7.0) of the solution, the surface attains a negative charge. Thus, an increase in the electrostatic attraction between a positively charged (cationic) dye and negatively charged adsorbent was achieved, resulting in an increase in adsorption [42,43]. The reason for the spectacular growth of the adsorption capacity from pH 10 to 11.1 could be due to the further increase in the dissociation degree of H^+ by the oxygen-containing functional groups at elevated pH, maximizing the electronegativity of the hydrochar and the electrostatic attractive force between the dye and hydrochar [44–46].

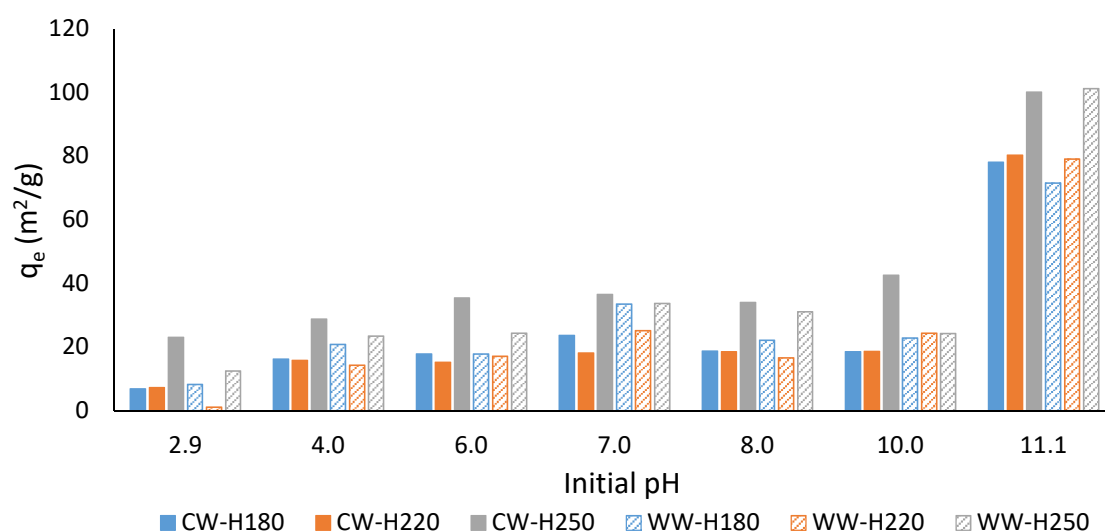


Figure 4. Effect of solution's pH on dye adsorption by hydrochars produced from citrus and winery wastes.

As all of the studied hydrochars have dominant acidic groups on the surface, the adsorption of a basic dye should be suitable. However, having different adsorption capacity indicates that the mechanism of adsorption on CW and WW hydrochars not only involves electrostatic attractions but also involves other interactions, such as pore filling, hydrogen bonding, or π - π interaction [32,40,47].

3.3. Adsorption Isotherms

The adsorption isotherm is an indication of the presence of adsorbate in the liquid (contaminated stream) and the solid (adsorbent) phases at a certain temperature. Investigating the adsorption isotherms will allow us to understand the type of adsorption whether it is monolayer adsorption (Langmuir) or multilayer adsorption (Freundlich). In this study, both the Langmuir and Freundlich models were investigated to describe the adsorption behavior of a cationic dye onto different hydrochar surfaces at three different adsorption temperatures. The adsorption isotherms for the hydrochars at different adsorption temperatures are shown in Figure 5. The corresponding parameters, such as the maximum adsorption capacity and Langmuir and Freundlich coefficients are also shown in Table 3. From Figure 5, it is clear that the adsorption capacity of both CW and WW decreased with the increase in their treatment temperature. For example, CW-H180 showed maximum adsorption capacity (Q_{max}) 66.23 mg/g at 4 °C, while CW-H250 showed 28.57 mg/g at the same adsorption temperature. A similar trend was followed by other samples in this study and is in accordance with what was

obtained when using sewage sludge hydrochars obtained at similar temperatures (namely: 190, 220, and 250 °C) for methylene blue adsorption [32]. The Q_{max} of the hydrochars exhibited the following order: CW-H180 > CW-H220 > CW-H250 and WW-H180 > WW-H220 > WW-H250 as shown in Table 3. In contrast, the BET surface areas were followed opposite trends CW-H250 > CW-H220 > CW-H180 and WW-H250 > WW-H220 > WW-H180 as shown in Table 2. These results demonstrate that other adsorption mechanisms are presented along with pore filling. In this case, the presence of oxygen functional groups could play a role. For example, both CW-H180 and WW-H180 have a lower amount of basic functional groups and a higher amount of carboxylic groups, which could favor the methylene blue adsorption, as it is a cationic or basic dye. In contrast, the basic groups increased with the HTC temperature while the carboxylic groups decreased which make the environment adverse to adsorb the dye as a result lower adsorption was observed at a higher temperature. In addition, the presence of lower functional groups per square meter of the hydrochar surface could be another reason for the lower adsorption.

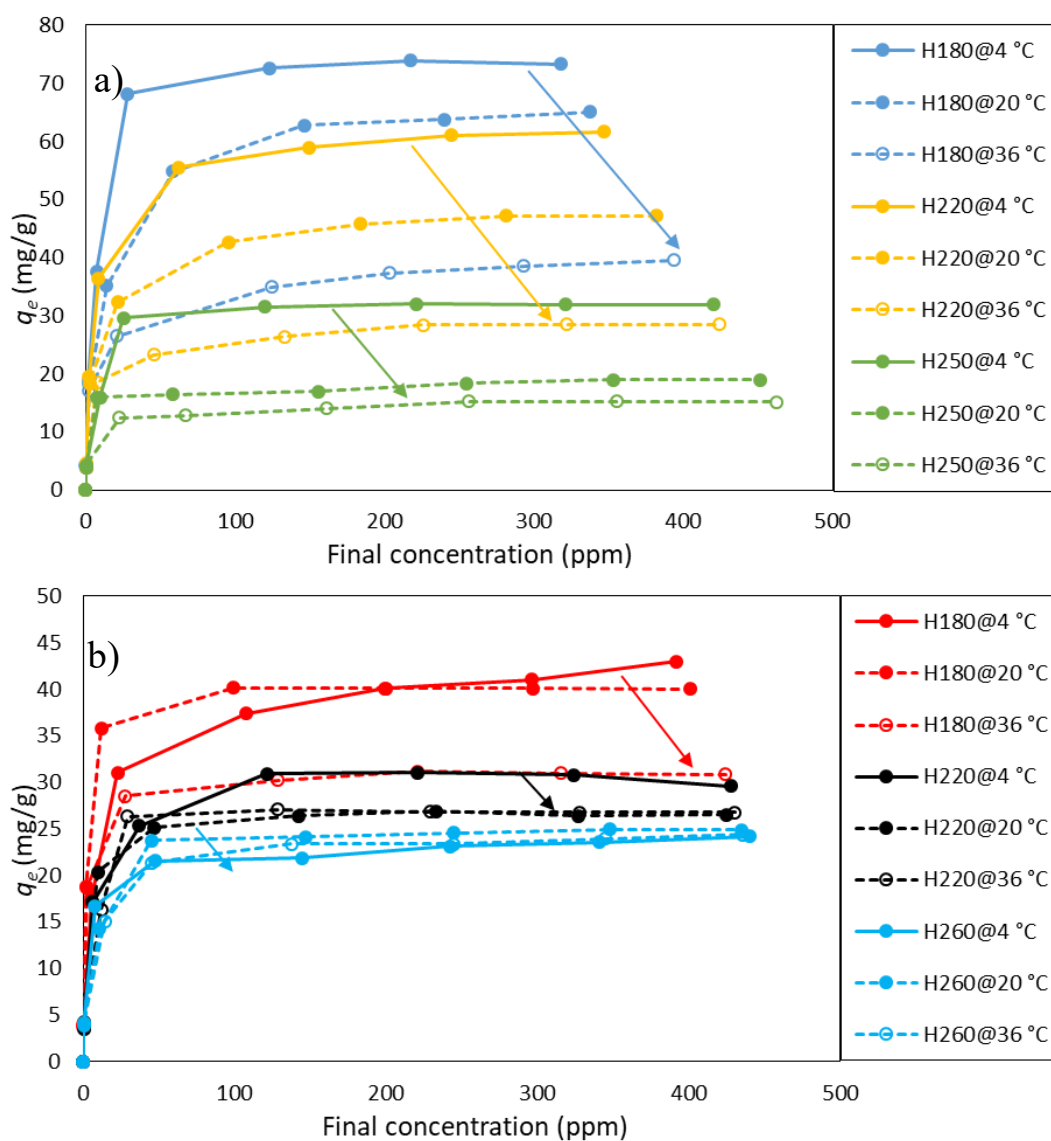


Figure 5. Equilibrium adsorption of dye at different temperatures on hydrochars produced from (a) citrus wastes, (b) winery wastes.

Table 3. Methylene blue adsorption by hydrochars produced from citrus and winery wastes: corresponding isotherm parameters from the Langmuir and Freundlich models.

Temperature (°C)	Sample ID	Langmuir Parameters			Freundlich Parameters		
		Q_{\max} (mg/g)	K_L	P^2	K_F	n_F	R^2
4	CW-H180	66.23	0.23	0.99	11.16	2.56	0.87
	CW-H220	60.24	0.21	0.99	10.15	2.79	0.86
	CW-H250	28.57	0.49	0.98	7.13	3.47	0.85
	WW-H180	36.63	0.29	0.99	7.42	3.04	0.89
	WW-H220	28.57	0.40	0.99	6.93	3.52	0.87
	WW-H250	22.83	0.46	0.99	6.55	4.13	0.84
20	CW-H180	51.02	0.34	0.99	9.72	2.68	0.92
	CW-H220	40.00	0.46	0.99	8.96	3.13	0.91
	CW-H250	17.89	1.24	0.99	6.86	5.34	0.82
	WW-H180	36.63	1.01	0.99	11.01	3.86	0.83
	WW-H220	25.97	0.64	0.99	6.99	3.85	0.85
	WW-H250	22.52	0.76	0.98	6.71	4.07	0.92
36	CW-H180	31.65	1.54	0.98	10.25	4.00	0.93
	CW-H220	25.64	1.10	0.99	8.30	4.33	0.92
	CW-H250	14.16	1.59	0.99	5.92	5.87	0.94
	WW-H180	28.65	1.96	0.99	9.64	4.36	0.85
	WW-H220	24.63	1.16	0.98	7.82	4.20	0.89
	WW-H250	21.69	1.11	0.98	6.82	4.25	0.94

Similarly to the HTC temperature, the adsorption capacity was strongly affected by the adsorption temperature shown in Figure 5 and Table 3. The operation temperatures also showed similar trends as the HTC temperature followed. WW-H250 showed a minimal effect (about 17%) of operation temperature on adsorption, while CW-H250 showed the maximum change (about 50%) in adsorption capacity. Although CW-H250 has the highest surface area among all studied samples, at the same time, it has the lowest density of functional groups which could be the determining factor of having the lowest adsorption capacity.

All the isotherms shown in Figure 5 were classified as L-type which corresponds to the Langmuir isotherm according to the classification. This type of isotherm is characterized by a decreasing slope with the increase in concentration as the vacant sites of the adsorbent decrease as it becomes covered by the adsorbate [48]. This adsorption behavior could also be explained by the high affinity of the adsorbent at low concentrations, which decreases further as concentration increases. The higher correlation coefficients (R^2) of the Langmuir model shown in Table 3 support this hypothesis. The equilibrium data were also fitted to the Freundlich equation and determined the parameters K_F and n_F . The R^2 values of the Freundlich model were found to be significantly lower than the Langmuir model. Ferrentino et al. observed a similar finding when using sewage sludge hydrochars obtained at similar temperatures [32]. All the values of dimensionless separation factor (R_L) shown in Table 4 fall between 0–1, which confirm the favorable uptake of the dye. Therefore, it can be concluded that the adsorption of a cationic dye onto CW and WW hydrochars mostly followed the Langmuir isotherm compared to the Freundlich isotherm. Moreover, the lower adsorption capacities at higher temperatures demonstrated that the dye removal process by the studied hydrochar could involve physical adsorption.

Although adsorption isotherms can contribute to revealing the adsorption mechanism, they are also useful in regards to obtaining thermodynamic parameters. The following section will discuss the thermodynamic parameters of dye adsorption onto CW and WW hydrochars.

Table 4. Separation factor of the Langmuir model.

Feedstock	Initial Conc. (ppm)	H180			H220			H250		
		4 °C	20 °C	36 °C	4 °C	20 °C	36 °C	4 °C	20 °C	36 °C
CW	10	0.998	0.997	0.985	0.998	0.995	0.989	0.995	0.988	0.984
	50	0.988	0.983	0.928	0.990	0.977	0.948	0.976	0.941	0.926
	100	0.977	0.967	0.866	0.980	0.956	0.901	0.953	0.889	0.863
	200	0.955	0.936	0.764	0.960	0.915	0.820	0.911	0.800	0.758
	300	0.934	0.907	0.684	0.941	0.878	0.752	0.872	0.728	0.677
	400	0.914	0.880	0.619	0.923	0.844	0.695	0.836	0.667	0.611
	500	0.895	0.854	0.565	0.906	0.812	0.645	0.803	0.616	0.557
WW	10	0.997	0.990	0.981	0.996	0.994	0.989	0.995	0.992	0.989
	50	0.986	0.952	0.911	0.981	0.969	0.945	0.978	0.964	0.947
	100	0.972	0.908	0.836	0.962	0.940	0.896	0.956	0.930	0.900
	200	0.946	0.831	0.718	0.927	0.887	0.811	0.916	0.869	0.818
	300	0.920	0.767	0.630	0.894	0.839	0.741	0.879	0.815	0.750
	400	0.897	0.711	0.560	0.863	0.797	0.682	0.845	0.768	0.692
	500	0.874	0.663	0.505	0.835	0.758	0.632	0.813	0.726	0.643

3.4. Adsorption Thermodynamics

The dye adsorption process could be either physical or chemical or both. The adsorption mechanism of a study is highly directed by its thermodynamic properties, such as ΔG , ΔS , and ΔH . The thermodynamic parameters of the adsorption process by CW and WW hydrochar are shown in Table 5. The results reveal that the adsorption phenomenon of both hydrochars occurred spontaneously, as the ΔG values at all temperatures are negative [49]. This finding agreed with the conclusions drawn from the separation factor (R_L) analysis described in the previous section, where all the values of RR_L varied between 0 and 1. The results also showed that the ΔG values decreased further about 20 to 25% and 18 to 25% for CW and WW, respectively, with the increase in adsorption temperature. Additionally, the ΔG values decrease with the increase in HTC temperature. These demonstrated that the adsorption on studied hydrochars was unfavorable at higher temperatures (both HTC and adsorption temperature). A similar observation was found by Tan et al. and Tran et al. where they studied the methylene blue and methylene green adsorption on activated carbon derived from oil palm fiber and hydrochars derived from golden shower pod, coconut shell, orange peel, respectively [50,51].

Table 5. Thermodynamic parameters for a dye adsorption process by hydrochars produced from citrus and winery wastes.

Sample ID	Temperature (°C)	Van't Hoff Equation	K_C	ΔG (KJ/mol)	ΔH (KJ/mol)	ΔS (J/mol)
CW-H180	4	$y = -4977.2x + 33.0$ $R^2 = 0.873$	4162272	-34.66	41.38	274.51
	20		6072126	-39.05		
	36		27363558	-43.44		
CW-H220	4	$y = -4452.3x + 31.2$ $R^2 = 0.997$	3681327	-34.77	37.02	259.14
	20		8233615	-38.91		
	36		19501840	-43.06		
CW-H250	4	$y = -3187.8x + 27.6$ $R^2 = 0.916$	8689631	-37.02	26.50	229.33
	20		22149969	-40.69		
	36		28290480	-44.36		
WW-H180	4	$y = -5154.8x + 34.1$ $R^2 = 0.978$	5112033	-35.75	42.90	283.93
	20		18015640	-40.29		
	36		34805250	-44.84		
WW-H220	4	$y = -2877.2x + 26.1$ $R^2 = 0.991$	7020436	-36.24	23.92	217.21
	20		11333988	-39.72		
	36		20650946	-43.19		
WW-H250	4	$y = -2369.4x + 24.5$ $R^2 = 0.998$	8141606	-36.67	19.70	203.50
	20		13427161	-39.93		
	36		19719331	-43.18		

The ΔH values varied between 41.38 to 26.50 KJ/mol and 42.90 to 19.70 KJ/mol for CW and WW hydrochar, respectively. All of these positive values indicate the adsorption process was endothermic in nature and not governed by the enthalpy [52]. As the process is not governed by the enthalpy, it should be governed by the entropy. The positive values of ΔS indicate that the adsorption of a cationic dye resulting in an increase in overall entropy in the system, which confirms the adsorption was entropy governed. The positive values of ΔS further indicated that the degree of freedom of dye increases in the solution, and the organization of the adsorbate at solid/liquid interface becomes more random during the adsorption process [40].

4. Conclusions

In this study, hydrochars were obtained from CW and WW via hydrothermal carbonization at 180, 220, and 250 °C. Thermodynamic properties of MB adsorption on those hydrochars were investigated including the adsorption isotherms at 4, 20, and 36 °C. The surface oxygen functionality and surface area were measured using Boehm titration and BET techniques, respectively. In addition, the chemical and electrical states of the hydrochar were measured. This study found that cation dye adsorption on CW and WW hydrochars followed Langmuir monolayer adsorption isotherm. The adsorption of MB on hydrochar is not only governed by the surface area but also the functional groups as well. It was observed that total oxygen functional groups remain similar (e.g., about 1080 and 1055 $\mu\text{mol/g}$ on CW and WW hydrochars, respectively) with the increase in HTC temperature from 180 to 250 °C, however, the specific functional groups reorganize with increasing HTC temperature. Although the surface area of the hydrochar increases with the HTC temperature for both feedstocks, the maximum adsorption capacity decreases from 66.23 to 28.57 mg/g and 36.63 to 22.83 mg/g at 4 °C for CW and WW, respectively because of the reduction of the density of the functional groups. In addition, if the adsorption follows the Langmuir isotherm, the functional group density is also important because it will determine how much active sites are available to adsorb the dye molecules. As Langmuir adsorption is essentially the monolayer adsorption, knowledge of the active sites per unit area of the hydrochar is necessary because it will control the adsorption capacity of the material. Therefore, it can be concluded from this study that both CW and WW worked best as adsorbent while they were treated at the lower temperature of 180 °C at which condition, both CW and WW hydrochars showed the highest active sites per unit area which translated in their best performances as adsorbent materials. Therefore, no further activation of these hydrochars is required.

This study provides a new direction of hydrochar application as adsorbent. For instance, industrial dyes are common water pollutants, especially for developing countries. Their adverse health effects on the peoples from low-income countries need to address with a low-cost solution that could be prepared from local resources. Activated carbon or synthetic adsorbent could be used for dye removal from water, however, these adsorbents are often expensive. This study presents the opportunity to utilize common agro-industrial wastes to adsorb industrial dyes from water.

Author Contributions: Conceptualization, M.V., N.S., R.V., and A.M.; methodology, N.S., M.V., A.M.; formal analysis, N.S., M.T.R., L.F., and R.V.; investigation, N.S., M.T.R., and M.V.; resources, M.V., R.V., and A.M.; writing—original draft presentation, N.S., M.T.R., and M.V., writing—review and editing, M.T.R., M.V., R.V., and L.F. All authors have read and agreed to the published version of the manuscript.

Funding: Part of the work is funded by the United States Department of Agriculture (USDA) grant (2019-67019-2928) through M.T.R.

Acknowledgments: The authors acknowledge Eric Guisbert and Alan Leonard from the department of Biomedical and Chemical Engineering and Sciences at Florida Institute of Technology for allowing to use their incubators. The authors are also thankful to Hannah Vest and Rosie Red from the Biofuels Lab at FIT for their laboratory efforts in this project.

Conflicts of Interest: The authors declare no conflict of interest.

References

1. Lazaroiu, G.; Mihaescu, L.; Negreanu, G.; Pana, C.; Pisa, I.; Cernat, A.; Ciupageanu, D.-A. Experimental investigations of innovative biomass energy harnessing solutions. *Energies* **2018**, *11*, 3469. [[CrossRef](#)]
2. Ronda, A.; Martín-Lara, M.A.; Calero, M.; Blázquez, G. Complete use of an agricultural waste: Application of untreated and chemically treated olive stone as biosorbent of lead ions and reuse as fuel. *Chem. Eng. Res. Des.* **2015**, *104*, 740–751. [[CrossRef](#)]
3. United States Department of Agriculture. *Citrus Fruits 2019 Summary*; United States Department of Agriculture: Washington, DC, USA, 2019.
4. International Organisation of Vine and Wine (OIV). *2019 Statistical Report on World Vitiviniculture*; Intergovernmental Organisation: New York, NY, USA, 2019.
5. Zacharof, M.-P. Grape winery waste as feedstock for bioconversions: Applying the biorefinery concept. *Waste Biomass Valorization* **2017**, *8*, 1011–1025. [[CrossRef](#)]
6. Martín, M.A.; Siles, J.A.; Chica, A.F.; Martín, A. Biomethanization of orange peel waste. *Bioresour. Technol.* **2010**, *101*, 8993–8999. [[CrossRef](#)]
7. Attard, T.M.; Watterson, B.; Budarin, V.L.; Clark, J.H.; Hunt, A.J. Microwave assisted extraction as an important technology for valorising orange waste. *New J. Chem.* **2014**, *38*, 2278–2283. [[CrossRef](#)]
8. Doymaz, İ.; Akgün, N. Study of thin-layer drying of grape wastes. *Chem. Eng. Commun.* **2009**, *196*, 890–900. [[CrossRef](#)]
9. Lavelli, V.; Torri, L.; Zeppa, G.; Fiori, L.; Spigno, G. Recovery of winemaking by-products for innovative food application. *Ital. J. Food Sci.* **2016**, *28*, 542–564.
10. Kebaili, M.; Djellali, S.; Radjai, M.; Drouiche, N.; Lounici, H. Valorization of orange industry residues to form a natural coagulant and adsorbent. *J. Ind. Eng. Chem.* **2018**, *64*, 292–299. [[CrossRef](#)]
11. Ciuta, S.; Antognoni, S.; Rada, E.C.; Ragazzi, M.; Badea, A.; Cioca, L.I. Respiriometric index and biogas potential of different foods and agricultural discarded biomass. *Sustainability* **2016**, *8*, 1311. [[CrossRef](#)]
12. Zhang, B.; Heidari, M.; Regmi, B.; Salaudeen, S.; Arku, P.; Thimmannagari, M.; Dutta, A. Hydrothermal carbonization of fruit wastes: A promising technique for generating hydrochar. *Energies* **2018**, *11*, 2022. [[CrossRef](#)]
13. Burguete, P.; Corma, A.; Hitzl, M.; Modrego, R.; Ponce, E.; Renz, M. Fuel and chemicals from wet lignocellulosic biomass waste streams by hydrothermal carbonization. *Green Chem.* **2016**, *18*, 1051–1060. [[CrossRef](#)]
14. Bandura, A.V.; Lvov, S.N. The ionization constant of water over wide ranges of temperature and density. *J. Phys. Chem. Ref. Data* **2006**, *35*, 15–30. [[CrossRef](#)]
15. Reza, M.T.; Rottler, E.; Herklotz, L.; Wirth, B. Hydrothermal carbonization (HTC) of wheat straw: Influence of feedwater pH prepared by acetic acid and potassium hydroxide. *Bioresour. Technol.* **2015**, *182*, 336–344. [[CrossRef](#)] [[PubMed](#)]
16. Sevilla, M.; Fuertes, A.B. The production of carbon materials by hydrothermal carbonization of cellulose. *Carbon* **2009**, *47*, 2281–2289. [[CrossRef](#)]
17. Fu, M.-M.; Mo, C.-H.; Li, H.; Zhang, Y.-N.; Huang, W.-X.; Wong, M.H. Comparison of physicochemical properties of biochars and hydrochars produced from food wastes. *J. Clean. Prod.* **2019**, *236*, 117637. [[CrossRef](#)]
18. Saha, N.; Saba, A.; Reza, M.T. Effect of hydrothermal carbonization temperature on pH, dissociation constants, and acidic functional groups on hydrochar from cellulose and wood. *J. Anal. Appl. Pyrolysis* **2019**, *137*, 138–145. [[CrossRef](#)]
19. Fang, J.; Gao, B.; Chen, J.; Zimmerman, A.R. Hydrochars derived from plant biomass under various conditions: Characterization and potential applications and impacts. *Chem. Eng. J.* **2015**, *267*, 253–259. [[CrossRef](#)]
20. Takaya, C.; Fletcher, L.; Singh, S.; Anyikude, K.; Ross, A. Phosphate and ammonium sorption capacity of biochar and hydrochar from different wastes. *Chemosphere* **2016**, *145*, 518–527. [[CrossRef](#)]
21. Román, S.; Nabais, J.M.V.; Laginhas, C.; Ledesma, B.; González, J.F. Hydrothermal carbonization as an effective way of densifying the energy content of biomass. *Fuel Process. Technol.* **2012**, *103*, 78–83. [[CrossRef](#)]
22. Zhou, Y.; Engler, N.; Li, Y.; Nelles, M. The influence of hydrothermal operation on the surface properties of kitchen waste-derived hydrochar: Biogas upgrading. *J. Clean. Prod.* **2020**, *259*, 121020. [[CrossRef](#)]

23. Basso, D.; Weiss-Hortala, E.; Patuzzi, F.; Baratieri, M.; Fiori, L. In deep analysis on the behavior of grape marc constituents during hydrothermal carbonization. *Energies* **2018**, *11*, 1379. [[CrossRef](#)]
24. Saba, A.; McGaughey, K.; Reza, T.M. Techno-Economic Assessment of Co-Hydrothermal Carbonization of a Coal-Miscanthus Blend. *Energies* **2019**, *12*, 630. [[CrossRef](#)]
25. Saha, N.; Saba, A.; Saha, P.; McGaughey, K.; Franqui-Villanueva, D.; Orts, W.J.; Hart-Cooper, W.M.; Reza, M.T. Hydrothermal carbonization of various paper mill sludges: An observation of solid fuel properties. *Energies* **2019**, *12*, 858. [[CrossRef](#)]
26. Erdogan, E.; Atila, B.; Mumme, J.; Reza, M.T.; Toptas, A.; Elibol, M.; Yanik, J. Characterization of products from hydrothermal carbonization of orange pomace including anaerobic digestibility of process liquor. *Bioresour. Technol.* **2015**, *196*, 35–42. [[CrossRef](#)] [[PubMed](#)]
27. Nascimento, G.E.d.; Duarte, M.M.M.B.; Campos, N.F.; Rocha, O.R.S.d.; Silva, V.L.d. Adsorption of azo dyes using peanut hull and orange peel: A comparative study. *Environ. Technol.* **2014**, *35*, 1436–1453. [[CrossRef](#)]
28. Fernandez, M.E.; Ledesma, B.; Román, S.; Bonelli, P.R.; Cukierman, A.L. Development and characterization of activated hydrochars from orange peels as potential adsorbents for emerging organic contaminants. *Bioresour. Technol.* **2015**, *183*, 221–228. [[CrossRef](#)]
29. Purnomo, C.W.; Castello, D.; Fiori, L. Granular activated carbon from grape seeds hydrothermal char. *Appl. Sci.* **2018**, *8*, 331. [[CrossRef](#)]
30. Zúñiga-Muro, N.M.; Bonilla-Petriciolet, A.; Mendoza-Castillo, D.I.; Reynel-Ávila, H.E.; Duran-Valle, C.J.; Ghalla, H.; Sellaoui, L. Recovery of grape waste for the preparation of adsorbents for water treatment: Mercury removal. *J. Environ. Chem. Eng.* **2020**, *8*, 103738. [[CrossRef](#)]
31. Singh, A.K.; Ketan, K.; Singh, J.K. Simple and green fabrication of recyclable magnetic highly hydrophobic sorbents derived from waste orange peels for removal of oil and organic solvents from water surface. *J. Environ. Chem. Eng.* **2017**, *5*, 5250–5259. [[CrossRef](#)]
32. Ferrentino, R.; Ceccato, R.; Marchetti, V.; Andreottola, G.; Fiori, L. Sewage Sludge Hydrochar: An Option for Removal of Methylene Blue from Wastewater. *Appl. Sci.* **2020**, *10*, 3445. [[CrossRef](#)]
33. Fiol, N.; Villaescusa, I. Determination of sorbent point zero charge: Usefulness in sorption studies. *Environ. Chem. Lett.* **2009**, *7*, 79–84. [[CrossRef](#)]
34. Tran, H.N.; You, S.-J.; Chao, H.-P. Effect of pyrolysis temperatures and times on the adsorption of cadmium onto orange peel derived biochar. *Waste Manag. Res.* **2016**, *34*, 129–138. [[CrossRef](#)] [[PubMed](#)]
35. Boehm, H.-P. Surface chemical characterization of carbons from adsorption studies. In *Adsorption by Carbons*; Elsevier: Amsterdam, The Netherlands, 2008; pp. 301–327.
36. Saha, N.; Xin, D.; Chiu, P.C.; Reza, M.T. Effect of pyrolysis temperature on acidic oxygen-containing functional groups and electron storage capacities of pyrolyzed hydrochars. *ACS Sustain. Chem. Eng.* **2019**, *7*, 8387–8396. [[CrossRef](#)]
37. Saha, N.; Reza, M.T. Effect of pyrolysis on basic functional groups of hydrochars. *Biomass Convers. Biorefinery* **2019**, 1–8. [[CrossRef](#)]
38. Tran, H.N.; You, S.-J.; Chao, H.-P. Thermodynamic parameters of cadmium adsorption onto orange peel calculated from various methods: A comparison study. *J. Environ. Chem. Eng.* **2016**, *4*, 2671–2682. [[CrossRef](#)]
39. Zhou, X.; Zhou, X. The unit problem in the thermodynamic calculation of adsorption using the Langmuir equation. *Chem. Eng. Commun.* **2014**, *201*, 1459–1467. [[CrossRef](#)]
40. Tran, H.N.; You, S.-J.; Chao, H.-P. Fast and efficient adsorption of methylene green 5 on activated carbon prepared from new chemical activation method. *J. Environ. Manag.* **2017**, *188*, 322–336. [[CrossRef](#)]
41. Arslan, Y.; Kendüzler, E.; Kabak, B.; Demir, K.; Tomul, F. Determination of Adsorption Characteristics of Orange Peel Activated with Potassium Carbonate for Chromium (III) Removal. *J. Turk. Chem. Soc. Sect. A Chem.* **2017**, *4*, 51–64.
42. Abd El-Latif, M.; Ibrahim, A.M. Adsorption, kinetic and equilibrium studies on removal of basic dye from aqueous solutions using hydrolyzed oak sawdust. *Desalin. Water Treat.* **2009**, *6*, 252–268. [[CrossRef](#)]
43. Boumediene, M.; Benaïssa, H.; George, B.; Molina, S.; Merlin, A. Effects of pH and ionic strength on methylene blue removal from synthetic aqueous solutions by sorption onto orange peel and desorption study. *J. Mater. Environ. Sci.* **2018**, *9*, 1700–1711.
44. Kuang, Y.; Zhang, X.; Zhou, S. Adsorption of methylene blue in water onto activated carbon by surfactant modification. *Water* **2020**, *12*, 587. [[CrossRef](#)]

45. Garg, V.K.; Gupta, R.; Bala Yadav, A.; Kumar, R. Dye removal from aqueous solution by adsorption on treated sawdust. *Bioresour. Technol.* **2003**, *89*, 121–124. [[CrossRef](#)]
46. Namasivayam, C.; Prabha, D.; Kumutha, M. Removal of direct red and acid brilliant blue by adsorption on to banana pith. *Bioresour. Technol.* **1998**, *64*, 77–79. [[CrossRef](#)]
47. Kermanioryani, M.; Mutalib, M.I.A.; Kurnia, K.A.; Lethesh, K.C.; Krishnan, S.; Leveque, J.-M. Enhancement of π - π aromatic interactions between hydrophobic Ionic Liquids and Methylene Blue for an optimum removal efficiency and assessment of toxicity by microbiological method. *J. Clean. Prod.* **2016**, *137*, 1149–1157. [[CrossRef](#)]
48. Sparks, D.L. *Environmental Soil Chemistry*; Elsevier: Amsterdam, The Netherlands, 2003.
49. Nasrullah, A.; Saad, B.; Bhat, A.H.; Khan, A.S.; Danish, M.; Isa, M.H.; Naeem, A. Mangosteen peel waste as a sustainable precursor for high surface area mesoporous activated carbon: Characterization and application for methylene blue removal. *J. Clean. Prod.* **2019**, *211*, 1190–1200. [[CrossRef](#)]
50. Tran, H.N.; You, S.-J.; Chao, H.-P. Insight into adsorption mechanism of cationic dye onto agricultural residues-derived hydrochars: Negligible role of π - π interaction. *Korean J. Chem. Eng.* **2017**, *34*, 1708–1720. [[CrossRef](#)]
51. Tan, I.; Hameed, B.; Ahmad, A. Equilibrium and kinetic studies on basic dye adsorption by oil palm fibre activated carbon. *Chem. Eng. J.* **2007**, *127*, 111–119. [[CrossRef](#)]
52. Dauenhauer, P.J.; Abdelrahman, O.A. A universal descriptor for the entropy of adsorbed molecules in confined spaces. *ACS Cent. Sci.* **2018**, *4*, 1235–1243. [[CrossRef](#)]



© 2020 by the authors. Licensee MDPI, Basel, Switzerland. This article is an open access article distributed under the terms and conditions of the Creative Commons Attribution (CC BY) license (<http://creativecommons.org/licenses/by/4.0/>).